

# Phase-Coupling-Induced Far-Field Modulation between Nontrivial and Trivial Modes in Cavity–Waveguide Systems

Xudong Zhan, Xiaofei Zang,\* Kun Liu, Jiong Xu, Yiming Zhu,\* and Songlin Zhuang

Photonic crystal (PhC) can be accurately designed to generate nontrivial and trivial modes, that is, edge states (ES)/corner states (CS) and cavity modes, respectively. The coupled cavity–waveguide system designed by PhC provides a chip-scale platform to manipulate electromagnetic (EM) waves that is usually based on near-field coupling between nontrivial and trivial modes. However, the far-field interaction between nontrivial and trivial modes for manipulating EM waves has not attracted wide attention yet. Herein this article, the coupled cavity–waveguide systems, which consist of two separated CS cavities (interacting with single/multiple trivial cavity/cavities) coupled by means of an ES waveguide, are designed to robustly tune the transmission properties of EM waves by modulating the phase coupling between CS cavities. As proof-of-principle examples, single-, dual-, and triple-electromagnetically-induced-transparency-like (EIT-like) phenomena with tunable transmission spectra are theoretically and numerically demonstrated by controlling the distance (generated phase accumulation) between the CS cavities. In addition, the robustness in generating EIT-like transmission characteristics is also demonstrated due to the robustness of the CS cavities. The unique cavity–waveguide systems with unprecedented capability in robustly tuning the transmission spectra of EM waves can be extended to design other high-performance devices with potential applications in sensing, detecting, and information processing.


trap light waves.<sup>[1]</sup> When waveguide and cavity are simultaneously introduced in a PhC, the coupled cavity–waveguide system can be designed to manipulate the transport of light. In the past two decades, a plethora of physical phenomena and practical applications such as Fano effects,<sup>[2,3]</sup> electromagnetically induced transparency,<sup>[4–6]</sup> sensors,<sup>[7,8]</sup> filters,<sup>[9–11]</sup> and all-optical buffers<sup>[12,13]</sup> have been demonstrated and realized based on the coupled cavity–waveguide systems. However, there are two main issues (in the traditional cavity–waveguide systems) that hinder the applications. One is the disorders (or defects) due to fabrication errors, which always lead to functional incapacitation of the aforementioned applications and phenomena. The other is that only the near-field coupling (between the waveguide and cavity [or between cavities]) is applied to the manipulation of electromagnetic (EM) waves, hindering further applications in coupled cavity–waveguide systems.

With further development of PhC accompanied by the topological understanding in condensed matter physics, the analogous photonic topological insulators (PTIs) have been proposed to robustly control EM waves.<sup>[14–20]</sup> ES, as one of the most remarkable properties of PTIs, enables the backscattering-immune functionality for guiding EM waves.<sup>[21–30]</sup> Usually, the  $n$ -dimensional PTIs have  $(n-1)$ -dimensional ES according to the bulk-boundary correspondence. Nevertheless, recent discovery of the higher-order topological insulators (HOTIs) goes beyond the traditional bulk-boundary correspondence, that is,  $n$ -dimensional HOTIs with  $(n-m)$ -dimensional ( $m > 1$ ) higher-order topological states.<sup>[31–45]</sup> The arising of HOTIs such as CS can be understood as the appearing of the quantization of nonzero higher-order multiple moments due to crystalline symmetries.<sup>[46,47]</sup> In comparison with a trivial cavity, the CS cavity enables stronger capability in robustly trapping EM waves.<sup>[48]</sup> When the ES waveguide and CS cavity/cavities are simultaneously integrated into a PhC, the topologically protected transmission (that is immune to the disorders or defects) and modulation of EM waves can be easily realized. For example, the coupled cavity (ES) waveguide enables the functionality in manipulating reflection-free transport of the photonic topological edge states (ESs).<sup>[48,49]</sup> The strong optical localization and high-quality-factor properties have been demonstrated in a coupled (CS)cavity–(ES) waveguide system.<sup>[50]</sup> In addition, an ES waveguide coupled with multiple cavities (e.g., a nontrivial cavity coupled with a trivial

## 1. Introduction

Photonic crystal (PhC or named as photonic bandgap materials), which consists of low-loss periodically dielectric structures, can prevent light of certain frequencies from propagating in any number of polarization directions.<sup>[1]</sup> By introducing line defects or point defects with the corresponding resonant frequencies in the bandgap, waveguides or cavities can be realized to guide or

X. Zhan, X. Zang, K. Liu, J. Xu, Y. Zhu, S. Zhuang  
Terahertz Technology Innovation Research Institute  
Terahertz Spectrum and Imaging Technology Cooperative Innovation Center  
Shanghai Key Lab of Modern Optical System  
University of Shanghai for Science and Technology  
No. 516 JunGong Road, Shanghai 200093, China  
E-mail: xfzang@usst.edu.cn; ymzhu@usst.edu.cn

 The ORCID identification number(s) for the author(s) of this article can be found under <https://doi.org/10.1002/adpr.202300089>.

© 2023 The Authors. Advanced Photonics Research published by Wiley-VCH GmbH. This is an open access article under the terms of the Creative Commons Attribution License, which permits use, distribution and reproduction in any medium, provided the original work is properly cited.

DOI: 10.1002/adpr.202300089

cavity) was proposed to generate EIT-like spectra that is robust to disorders.<sup>[51]</sup> However, the previous works are mainly focused on the near-field coupling (between the waveguide and cavity) for the robustness of optical control and manipulation. The far-field coupling (i.e., the phase coupling between two separated CS cavities), which can be considered as a new degree of freedom, for manipulating EM waves hasn't attracted wide attention yet.

In this article, the phase coupling between two separated CS cavities is proposed as a new avenue to robustly tuning the transport properties of EM waves. The PhC-based cavity-waveguide systems consisting of two separated CS cavities (and single/multiple trivial cavity/cavities) coupled with an ES waveguide are designed, and the single-, dual-, and triple-EIT-like phenomena with tunable transmission spectra are numerically demonstrated by controlling the distance (induced phase accumulation) between two CS cavities. The robust characteristics (that are immune to disorders) of EIT-like spectra are also investigated. In addition, theoretical models are constructed to further reveal/prove the tunable properties of the transmission spectra in the designed cavity-waveguide systems.

## 2. Principle and Design

The designed cavity-waveguide system is schematically shown in **Figure 1a**, which consists of two separated CS cavities (and a trivial cavity coupled with the left CS cavity) coupled with an ES

waveguide. The structure parameters designed in the cavity-waveguide system are as follows: the lattice constant ( $a$ ) of the PhC is 20 nm.  $d_1$  and  $d_2$  are 4.64 and 3.888 nm, respectively. The permittivity of dielectric rods is  $\epsilon_d = 9.5$ , while the background index is  $n_a = 1.0$ . The projected band of the combined PhC (of PhC1 [consisting of periodic unit cells of UC1] and PhC3 [consisting of periodic unit cells of UC3]) is shown in the inset of **Figure 1b**, and one-way ESs can be observed. For example, **Figure 1b** shows the electric-field ( $E_z$ ) distribution under the illumination of left-handed circularly-polarized orbital-angular momentum (OAM) source in the designed ES waveguide, and the excited ES mode can only propagate into the right side without back-reflection (see the detailed discussions in **Figure S1**, Supporting Information). For the incidence of RCP OAM source, the excited ES mode can only propagate into the left side without back-reflection (which is not shown here). The Zak phase of the combined PhC (PhC1 and PhC3) are quantized as 0 or  $\pi$ , which can be obtained by numerically calculating symmetric properties of electric field at high symmetry points in the Brillouin zone (see the calculated electric-field distributions in **Figure S2**, Supporting Information). The Zak phase of PhC1 is (0, 0), while it is (0,  $\pi$ ) for PhC3. As a result, there will be edge state(s) in the bandgap of this combined PhC (PhC1 and PhC3) due to the bulk-edge correspondence. Furthermore, when PhC2 surrounded by PhC1, the corner state (CS) can be excited shown in **Figure 1c**, since the Zak phase of PhC2 is ( $\pi$ ,  $\pi$ ). The trivial cavity is introduced in PhC1 by shifting rods in four neighboring unit cells

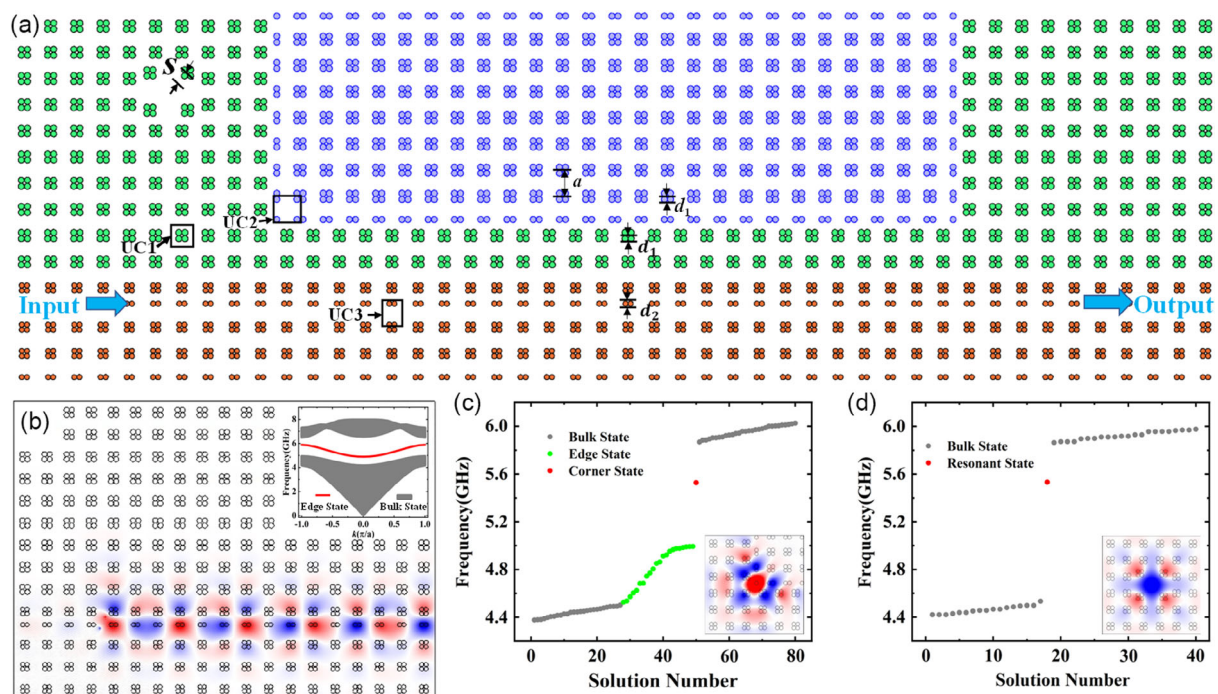


**Figure 1.** Schematic, eigenmodes, and electric-field distributions ( $E_z$ ) of the cavity-waveguide system consisting of two separated corner-state (CS) cavities (and a trivial cavity coupled with the left CS cavity) coupled with an edge-state (ES) waveguide. a) Schematic of the cavity-waveguide system; b) the ES excited in the designed waveguide. Inset shows the projected band of photonic crystal (PhC)1 (consisting of periodic unit cells of UC1) and PhC3 (consisting of periodic unit cells of UC3). The excited frequency of ES is 5.5082 GHz. c) Eigenmodes excited in the structure consisting of PhC2 (consisting of periodic unit cells of UC2) and PhC1. Inset shows the CS eigenmode in the CS cavity. The excited frequency of CS is 5.5270 GHz. d) Eigenmodes excited in the structure consisting of PhC1 with a point defect. Inset shows the resonant cavity mode in the trivial cavity. The excited frequency of trivial cavity is 5.5321 GHz.

(along the diagonal and antidiagonal directions with shifting distance of 4.3312 mm), and the corresponding eigenmodes and resonant cavity mode are shown in Figure 1d. It should be noted that the spatial distribution of the localized CS in both directions ( $x$ - and  $y$ -direction) is about  $2a$  (the length of two lattices), which means that the excited CS mode is highly located in the corner. Therefore, when the distance between the two CS cavities (shown in Figure 1a) is much more than  $2a$  (e.g.  $26a$ ), both of CS cavities cannot be directly coupled with each other, and thus, these two CS cavities can be indirectly coupled with each other by the phase coupling between them (see the detailed discussions in Figure S3, Supporting Information). Such a phase coupling can be considered as the far-field interaction between these two CS cavities.

### 3. Results

As a feasibility study, a cavity–waveguide system consisting of only two separated CS cavities coupled by means of an ES waveguide is designed to manipulate transmission properties of EM waves. The theoretical schematic of such a cavity–waveguide system is shown in Figure 2a. The Hamiltonian of a CS cavity (i.e., cavity 1 [ $C_1$ ] in Figure 2a) coupled with an ES waveguide can be governed by

$$H = \int dx C_R^\dagger(x) \left( \omega_0 - iv_g \frac{\partial}{\partial x} \right) C_R(x) + C_L^\dagger(x) \left( \omega_0 + iv_g \frac{\partial}{\partial x} \right) C_L(x) + \int dx V_1 \delta(x) \times [C_R^\dagger(x)c_1 + C_L^\dagger(x)c_1] + \omega_{c_1} c_1^\dagger c_1 + h.c. \quad (1)$$

where  $C_L^\dagger(x)$  (or  $C_R^\dagger(x)$ ) is creation operator of the left-moving (or right-moving) of ES, and  $v_g$  is group velocity of ES.  $V_1 (= V_2)$  illustrates the coupling between the waveguide and cavity 1 (2).  $\omega_{c_1}$  is the resonant frequency of cavity 1 ( $C_1$ ). The stationary eigenstate of the Hamiltonian can be given by

$$H|\Phi\rangle = \left[ \int dx \varphi_R(x, t) C_R^\dagger(x) + \varphi_L(x, t) C_L^\dagger(x) + \varphi_{c_1}(t) c_1^\dagger \right] \cdot |\emptyset\rangle \quad (2)$$

where  $\varphi_L(x)$  ( $\varphi_R(x)$ ) is the wave function of left-moving (right-moving) of ES in the waveguide, while  $\varphi_{c_1}$  is the wave function of cavity 1.  $|\emptyset\rangle$  is a vacuum state.

The transmission coefficient ( $t$ ) of the designed cavity–waveguide system consisting an ES waveguide coupled with a CS cavity can be deduced from the following equation

$$H|\Phi\rangle = i\hbar \frac{\partial}{\partial t} |\Phi\rangle \quad (3)$$

The transmitted and reflected coefficients can be deduced by solving Schrödinger equation

$$\begin{cases} t_1 = \frac{\omega - \omega_{c_1}}{\omega - \omega_{c_1} + i \frac{V_1^2}{v_g}} \\ r_1 = \frac{-i \frac{V_1^2}{v_g}}{\omega - \omega_{c_1} + i \frac{V_1^2}{v_g}} \end{cases} \quad (4)$$

It should be noted that the transmitted and reflected coefficients can be also deduced from the common coupled mode

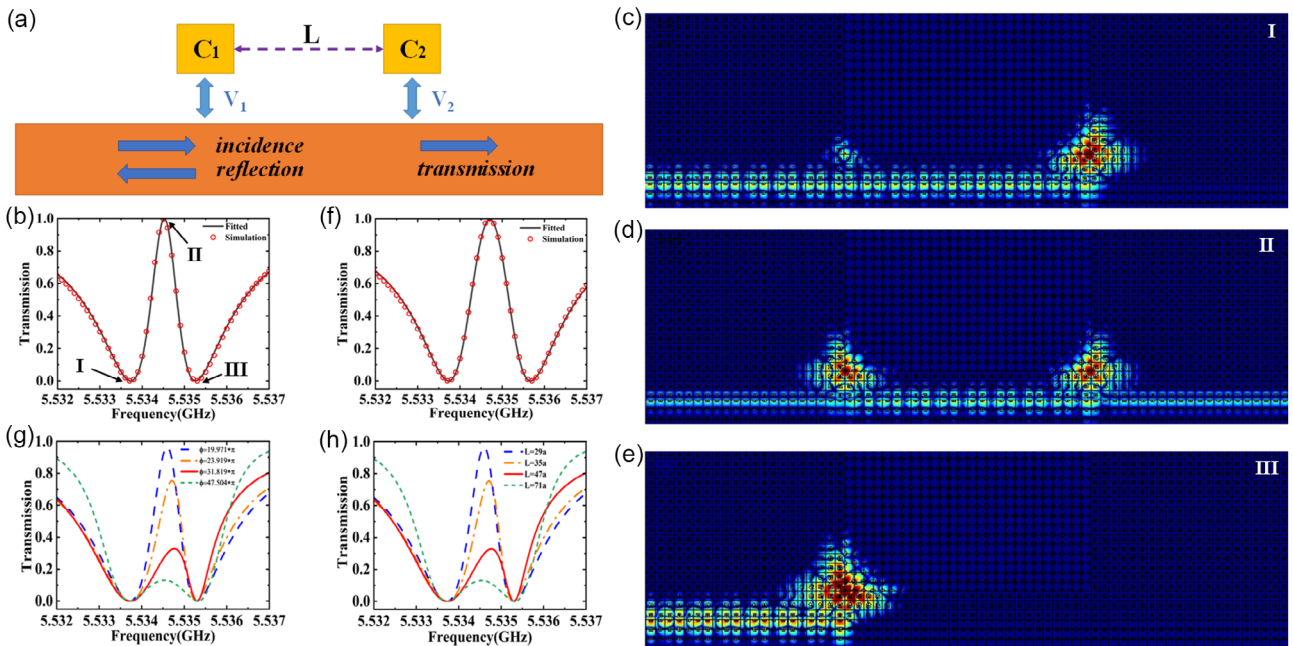


**Figure 2.** a) Theoretical model of the cavity–waveguide system consisting of two separated CS cavities coupled by an ES waveguide. b) The fitted (from the theoretical model) and simulated transmission spectra of the designed cavity–waveguide system (with  $\varphi = kL$ ). c–e) The calculated electric-field intensity distributions at I (5.5337 GHz), II (5.5345 GHz), and III (5.5353 GHz), respectively. f) The fitted (from the theoretical model) and simulated transmission spectra of the designed cavity–waveguide system (with  $\varphi = kL$ ) by embedding disorders. g) The theoretical and h) simulated spectra with different far-field couplings of  $\theta (= 2\varphi)$ .



equations.<sup>[52,53]</sup> To obtain an EIT-like transmission spectrum, the left CS cavity should be detuned from the right CS cavity. In simulation, one needs to appropriately reduce the diameter of the rod in the diagonal direction of the left corner (schematic in Figure S4, Supporting Information). For the cavity–waveguide system consisting of two separated CS cavities (with far-field coupling) coupled by an ES waveguide, the transfer matrix  $M$  (of such system)<sup>[54,55]</sup> is determined by

$$M = \begin{pmatrix} \frac{(t_1^2 - r_1^2)}{t_1} & \frac{r_1}{t_1} \\ -\frac{r_1}{t_1} & \frac{1}{t_1} \end{pmatrix} \begin{pmatrix} e^{i\varphi} & 0 \\ 0 & e^{-i\varphi} \end{pmatrix} \begin{pmatrix} \frac{(t_2^2 - r_2^2)}{t_2} & \frac{r_2}{t_2} \\ -\frac{r_2}{t_2} & \frac{1}{t_2} \end{pmatrix} \quad (5)$$

where  $\varphi = k \cdot L$  ( $L$  is the distance between two CS cavities while  $k$  is defined as the propagation constant in the ES waveguide).  $\omega_{c_2}$  is the resonant frequency of cavity 2 ( $C_2$ ). The transmission and reflection coefficients of  $t_2$  and  $r_2$  can be written as follows

$$\begin{cases} t_2 = \frac{\omega - \omega_{c_2}}{\omega - \omega_{c_2} + i \frac{V_2^2}{v_g}} \\ r_2 = \frac{-i \frac{V_2^2}{v_g}}{\omega - \omega_{c_2} + i \frac{V_2^2}{v_g}} \end{cases} \quad (6)$$

The transmitted intensity of the combined system with two separated CS cavities coupled by an ES waveguide can be defined as

$$T = \left| \frac{1}{M_{22}} \right|^2 = \left| \frac{t_1 t_2}{1 - r_1 r_2 \exp(2i\varphi)} \right|^2 \quad (7)$$

According to Equation (7), an EIT-like transmission spectrum with one peak (at 5.5345 GHz) and two dips (at 5.5337 and 5.5353 GHz) is observed, as shown in Figure 2b (black curve). The simulated result is also shown in Figure 2b (see the red curve), which is well matched with the fitted curve (the distance between two separated CS cavities is  $26a$ ). The electric-field intensity distributions at I, II, and III are shown in Figure 2c, d, e, respectively. As illustrated in Figure 2c, the left dip is caused by the resonance of the right CS cavity, while the right dip can be attributed to the resonance of the left CS cavity (see Figure 2e). The transparent peak is induced by destructive interference between the two CS cavities. Although the traditionally coupled cavity–waveguide system (which consists of two separated trivial cavities coupled with a waveguide) can also generate such an EIT-like transmission spectrum (Figure S5, Supporting Information), it is limited to disorders (due to fabrication errors). However, the proposed cavity–waveguide system can enable the disorder-immune functionality due to the robustness of CS. As a proof-of-principle example, the disorder is embedded into the designed cavity–waveguide system by shifting a rod that is in the diagonal direction of the left CS cavity schematic in Figure S6a, Supporting Information). The shifting distance is  $d = a/4 = 5$  mm, while the calculated transmission spectrum is shown in Figure 2f. As demonstrated in Figure 2f, an EIT-like transmission spectrum is also observed with one peak (at 5.5346 GHz) and two dips (at 5.5337 and 5.5357 GHz) (The corresponding electric-field intensity distributions in I, II, and III are supplied in Figure S6c, d, e, Supporting

Information). In this situation, the frequency detuning of the left CS cavity with and without disorder is only 0.0004 GHz, leading to trifling impact on the transmission spectrum. In contrast, for the traditional cavity–waveguide system consisting of two separate trivial cavities coupled with a trivial waveguide, the EIT-like transmission spectrum is disappeared due to the disorder (see the schematic and the corresponding transmission spectrum and electric-field distributions in Figure S6f–j, Supporting Information). The frequency detuning of the left trivial cavity with and without disorder is 0.1014 GHz, which can be considered as a strong detuning (from the left trivial cavity), resulting in the disappearance of the EIT-like phenomenon. Therefore, the designed cavity–waveguide system in this work enables the robust capability in generating EIT-like transmission spectrum.

The proposed approach for the designed cavity–waveguide system cannot only robustly manipulate EM waves, but also enables the functionality in tuning the transmission spectrum. According to Equation (7), the transmitted intensity can be tuned by accurately controlling the phase coupling between the CS cavities: In fact, the transmitted intensity in the theoretical model is determined by the phase coupling ( $2\varphi$ ) when the other parameters ( $t_1$ ,  $t_2$ ,  $r_1$ , and  $r_2$ ) are fixed. And thus, one can tune the transmission spectrum just by controlling the phase coupling (induced by the distance) between the two separated CS cavities. Figure 2g shows the transmission spectra of the designed cavity–waveguide system with different phase coupling. For  $\varphi = 19.971\pi$ , the transmissivity of the transparent peak is  $T = 95\%$  (see blue curve in Figure 2g). When  $\varphi = 23.919\pi$ ,  $31.819\pi$ , and  $47.504\pi$ , the transmissivity of the transparent peak is  $T = 75\%$ ,  $32\%$ , and  $12\%$  (see the orange, red, and green curves in Figure 2g), respectively. In a word, the transparent peak can be theoretically tuned from 100% to 12% just by the control phase coupling between two separated CS cavities. Therefore, an EM-waves-based switch can be realized by modulating the phase coupling between  $17.994\pi$  and  $47.504\pi$ , respectively (see Figure 2b and green curve in Figure 2g). The calculated results are shown in Figure 2h. It can be observed that the calculated transmissivity of transparent peak can be also gradually tuned by controlling the distance (that is the phase coupling) between these two separated CS cavities. The calculated results are matched with the theoretical model, which demonstrates that the phase coupling (between the two separated CS cavities) can be well applied to tune the transmission spectrum of the designed cavity–waveguide system. When a defect is introduced nearby the right CS cavity, the single-EIT-like transmission spectrum can be also obtained, as shown in Figure S7, Supporting Information.

When a trivial cavity is introduced and coupled with the left CS cavity (see the schematic in Figure 1a), a dual-EIT-like spectrum can be obtained, and the corresponding two transparent peaks can be flexibly tuned based on the phase coupling between the two separated CS cavities. By shifting the rods of four neighboring unit cells (in both diagonal and antidiagonal directions) in PhC1, a trivial cavity is introduced in the cavity–waveguide system and directly coupled with the left CS cavity. Figure 3a shows the theoretical model of such a cavity–waveguide system. The Hamiltonian of a CS cavity (i.e., cavity 1 [ $C_1$ ] in Figure 3a) coupled with an ES waveguide and a trivial cavity (e) can be depicted by

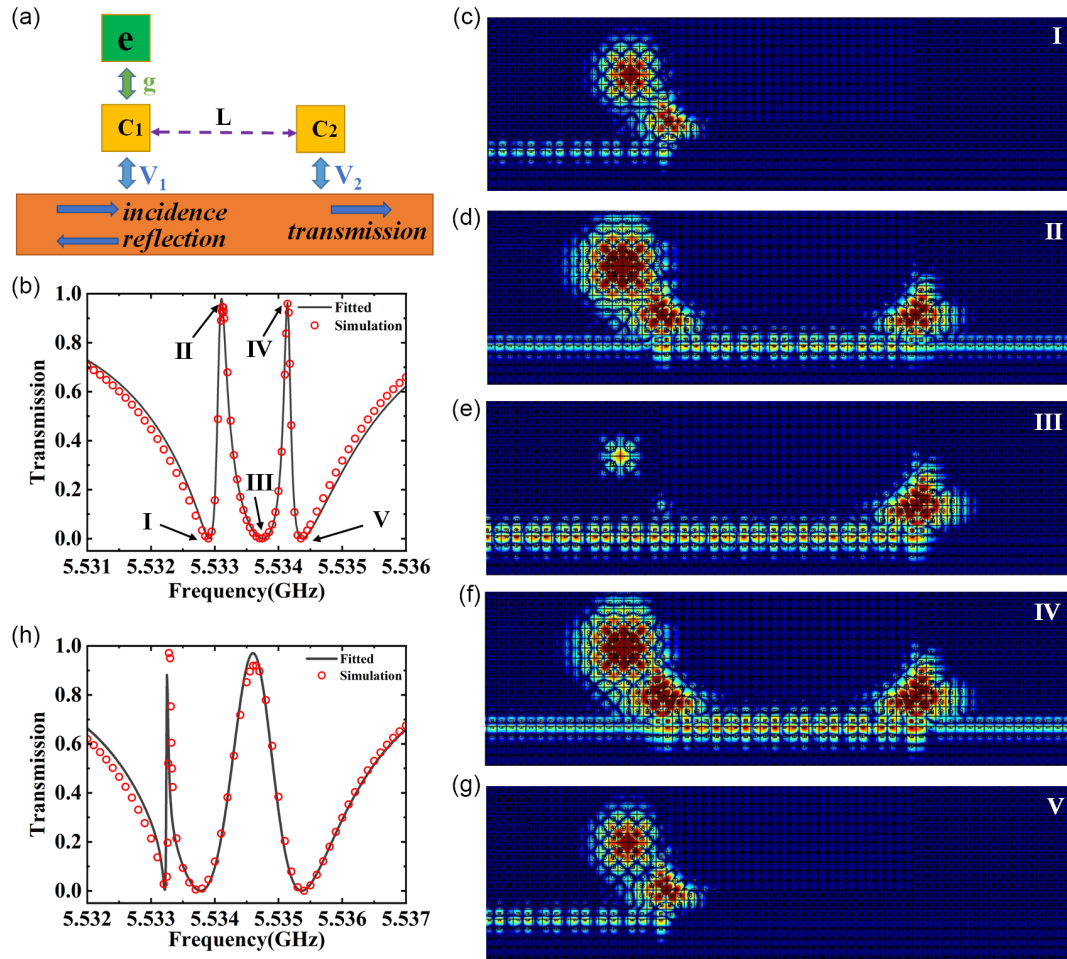


**Figure 3.** a) The theoretical model of a cavity–waveguide system consisting of one trivial cavity and two separated CS cavities coupled by an ES waveguide. b) The fitted (from the theoretical model) and simulated transmission spectra of the designed cavity–waveguide system with  $\varphi = k \cdot L \approx 18.016\pi$ . c–g) The calculated electric-field intensity distributions at I (5.53291 GHz), II (5.53312 GHz), III (5.53372 GHz), IV (5.53414 GHz), and V (5.53435 GHz), respectively. h) The fitted (from the theoretical model) and simulated transmission spectra of the designed cavity–waveguide system (with  $\varphi = k \cdot L \approx 18.016\pi$ ) by embedding disorders.

$$\begin{aligned}
 H = & \int dx C_R^\dagger(x) \left( \omega_0 - i\nu_g \frac{\partial}{\partial x} \right) C_R(x) \\
 & + C_L^\dagger(x) \left( \omega_0 + i\nu_g \frac{\partial}{\partial x} \right) C_L(x) + \int dx V_1 \delta(x) \\
 & \times [C_R^\dagger(x)c_1 + C_L^\dagger(x)c_1] + \omega_{c_1} c_1^\dagger c_1 + \omega_e e^\dagger e + g c_1^\dagger e + h.c.
 \end{aligned} \quad (8)$$

where  $C_e^\dagger$  ( $C_e$ ) is the creation (annihilation) operator of the trivial cavity with the corresponding eigenfrequency of  $\omega_e$ ,  $g$  is the coupling between the cavity  $e$  and the left CS cavity. The eigenstate of this Hamiltonian can be written as

$$\begin{aligned}
 |\Phi\rangle = & \left[ \int dx \varphi_R(x, t) C_R^\dagger(x) + \varphi_L(x, t) C_L^\dagger(x) \right. \\
 & \left. + \varphi_{c_1}(t) c_1^\dagger + \varphi_e(t) e^\dagger \right] \cdot |\emptyset\rangle
 \end{aligned} \quad (9)$$

The transmitted and reflected coefficients can be obtained by solving the Equation (3).

$$\begin{cases} t_1 = \frac{(\omega - \omega_e)(\omega - \omega_{c_1}) - g^2}{(\omega - \omega_e)(\omega - \omega_{c_1} + i\frac{V_1^2}{v_g^2}) - g^2} \\ r_1 = \frac{-(\omega - \omega_e)i\frac{V_1^2}{v_g^2}}{(\omega - \omega_e)(\omega - \omega_{c_1} + i\frac{V_1^2}{v_g^2}) - g^2} \end{cases} \quad (10)$$

The transmitted intensity of the combined system can be also illustrated like in Equation (7) (the transmitted and reflected coefficients of  $t_2$  and  $r_2$  are the same as Equation (6)).

In theory, the destructive interference between two CS cavities can induce a transparent peak, while the destructive interference between the trivial cavity and the left CS cavity can also generate a transparent peak, leading to a dual-EIT-like transmission spectrum. The fitted transmission spectrum from the theoretical model (see Equation (7)) is shown in Figure 3b (see the black curve). There are two peaks (at 5.53312 and 5.53414 GHz) and three dips (at 5.53291, 5.53372, and 5.53435 GHz) appeared in the corresponding transmission spectrum. The numerically

calculated result is also shown in Figure 3b (see the red curve), and both the fitted and calculated results are matched with each other. The corresponding electric-field intensity distributions at points I–V are shown in Figure 3c–g. The two dips at 5.53291 and 5.53435 GHz are caused by the constructive interference between the trivial cavity and the left CS cavity (see Figure 3c,g). The dip at 5.53372 GHz is due to the resonance of the right CS cavity (see Figure 3e). The two peaks at 5.53312 and 5.53414 GHz are generated due to the destructive interference between the trivial cavity and two CS cavities (the dual-EIT-like transmission spectrum can be also generated in a cavity–waveguide system consisting an ES waveguide coupled with two separated trivial cavities [Figure S8, Supporting Information]). The designed cavity–waveguide system (see Figure 1a) can also enable the disorder–immune functionality due to the robustness of CS. By embedding a disorder (i.e., by shifting a rod in the diagonal direction of the left CS cavity with shifting distance of  $a/4 = 5$  mm (schematic in Figure S9a, Supporting Information) into the cavity–waveguide system, the theoretical and calculated dual-EIT-like transmission spectrum is also maintained, as shown in Figure 3h (the electric-field intensity distributions in Figure S9c–g, Supporting Information). Although the traditional cavity–waveguide system (i.e., a waveguide is directly coupled with two separated trivial cavities and the left trivial cavity is directly coupled with another trivial cavity) can generate dual-EIT-like transmission spectrum (see Figure S8b, Supporting Information), the dual-EIT-like transmission spectrum is disappeared when the disorder (i.e., by shifting a rod in the diagonal direction of the left trivial cavity with shifting distance of  $a/4 = 5$  mm [the schematic in Figure S9h, Supporting Information]) is introduced in the system (Figure S9i–n, Supporting Information). According to Equation (7), the transmitted intensity in such a cavity–waveguide system (consisting of two separated CS cavities, a trivial cavity and an ES waveguide) is also determined by the phase coupling between the two separated CS cavities. As shown by Figure 3d,f for two transparent peaks, the generation mechanism of the two peaks is the destructive interference between two separated CS cavities and the trivial cavity, and thus, the adjustment of the distance (between the two CS cavities) will simultaneously modulate the transmissivity of these two peaks, as shown in **Figure 4**. When the distance between the two CS cavities is  $29a$ , the theoretical (simulated) transmissivity of the cavity–waveguide system at 5.53314 and 5.53418 GHz are 81.3% and 86.5% (79.6% and 87.4%) (see Figure 4a1,b1), respectively, which are lower than that of  $L = 26a$  (see Figure 3b). It shows that the enhancement of distance (between the two CS cavities) can simultaneously modulate the transmissivity of these two peaks. When the distance (between the two CS cavities) is switched from  $L = 32a$  to  $L = 77a$ , the transmissivity for two peaks are gradually reduced and less than 9.6%, as shown in Figure 4a2–b5. For  $L = 77a$ , the two peaks are nearly disappeared, leading to a band-stop filter. In a word, the designed cavity–waveguide system enables capability in simultaneously manipulate two transparent peaks in the dual-EIT-like transmission spectrum. When a defect is introduced nearby the right CS cavity, the dual-EIT-like transmission spectrum can be also obtained, as shown in Figure S10, Supporting Information.

When another trivial cavity is symmetrically introduced and coupled with the right CS cavity, a cavity–waveguide system consisting of two separated CS cavities (and each CS cavity is directly coupled

with a trivial cavity) coupled by means of an ES waveguide is designed to robustly manipulate the propagation of EM waves (the schematic in Figure S11a, Supporting Information). The transmitted intensity is the same as Equation (7), while the transmitted and reflected coefficients of  $t_1$ ,  $t_2$ ,  $r_1$ , and  $r_2$  can be expressed as

$$\begin{cases} t_i = \frac{(\omega - \omega_{e_i})(\omega - \omega_{c_i}) - g^2}{(\omega - \omega_{e_i})(\omega - \omega_{c_i} + i\frac{V_i^2}{v_g^2}) - g^2} \\ r_i = \frac{-(\omega - \omega_{e_i})i\frac{V_i^2}{v_g^2}}{(\omega - \omega_{e_i})(\omega - \omega_{c_i} + i\frac{V_i^2}{v_g^2}) - g^2} \end{cases} \quad (11)$$

where  $i = 1, 2$ ,  $\omega_{e_1} = \omega_{e_2} = \omega_e$ , and  $\omega_{c_1} = \omega_{c_2} = \omega_c$ . In this case, the left and right CS cavity coupled with a trivial cavity can be considered as two identical mirrors, and thus, a Fabry–Pérot interferometer consisting of an ES waveguide and two identical mirrors is constructed (see the theoretical model in **Figure 5a**). For  $\varphi = k \cdot L \neq n\pi$  ( $n$  is integer), there will be three peaks (and four dips) appeared in the transmission spectrum of the designed system, resulting in the triple-EIT-like phenomenon (the corresponding electric-field intensity distributions of three peaks are provided in Figure S11c–e, Supporting Information [for  $L = 32a$ ]). The transmission properties of the triple-EIT-like phenomenon based on trivial cavities coupled with an ES waveguide are provided in Figure S11, Supporting Information. The robust properties of our designed cavity–waveguide system are also demonstrated in Figure S12, Supporting Information. When  $\omega = \omega_e$ , the left and right mirrors are completely transparent with respect to the incident EM waves, and thus, the middle transparent peak (at  $\omega = \omega_e = 5.5335$  GHz) cannot be affected by the changing the distance between the two CS cavities, since the incident EM waves is completely transmitted from each mirror without reflection. For  $\omega \neq \omega_e$ , the originally mirrors can be regarded as two partially reflective mirrors, and the forward and backward EM waves located between two CS cavities can be interfered with each other, leading to two sharply side-peaks. The two sharp side-peaks result from the constructive interference of the forward and backward EM waves in the designed Fabry–Pérot interferometer (resulting from the two partially reflective mirrors). In other words, the appearance of the two sharply side-peaks is totally caused by the phase coupling between two CS cavities, and thus, one can easily modulate the two sharp side-peaks by controlling the distance between the two CS cavities. As shown in Figure 5, for the distance  $L$  switched from  $32a$  to  $38a$ ,  $47a$ , and  $56a$ , the transmissivity for the second and fourth dips are gradually increased, and the two sharp side-peaks are disappeared for  $L = 77a$ , leading to a single-EIT-like transmission spectrum. Therefore, the two sharply side-peaks induced by interference can be tuned easily by controlling the phase coupling between the two CS cavities, while the middle transparent peak is fixed (untuned) due to the completely transparent characteristic of each mirror (consisting of a CS cavity coupled with a trivial cavity). Therefore, a dual-frequency switch (due to the tunable transmission spectra of the two side-peaks) can be realized just by controlling the distance between the two CS cavities. When a defect is introduced nearby the right CS cavity, the triple-EIT-like

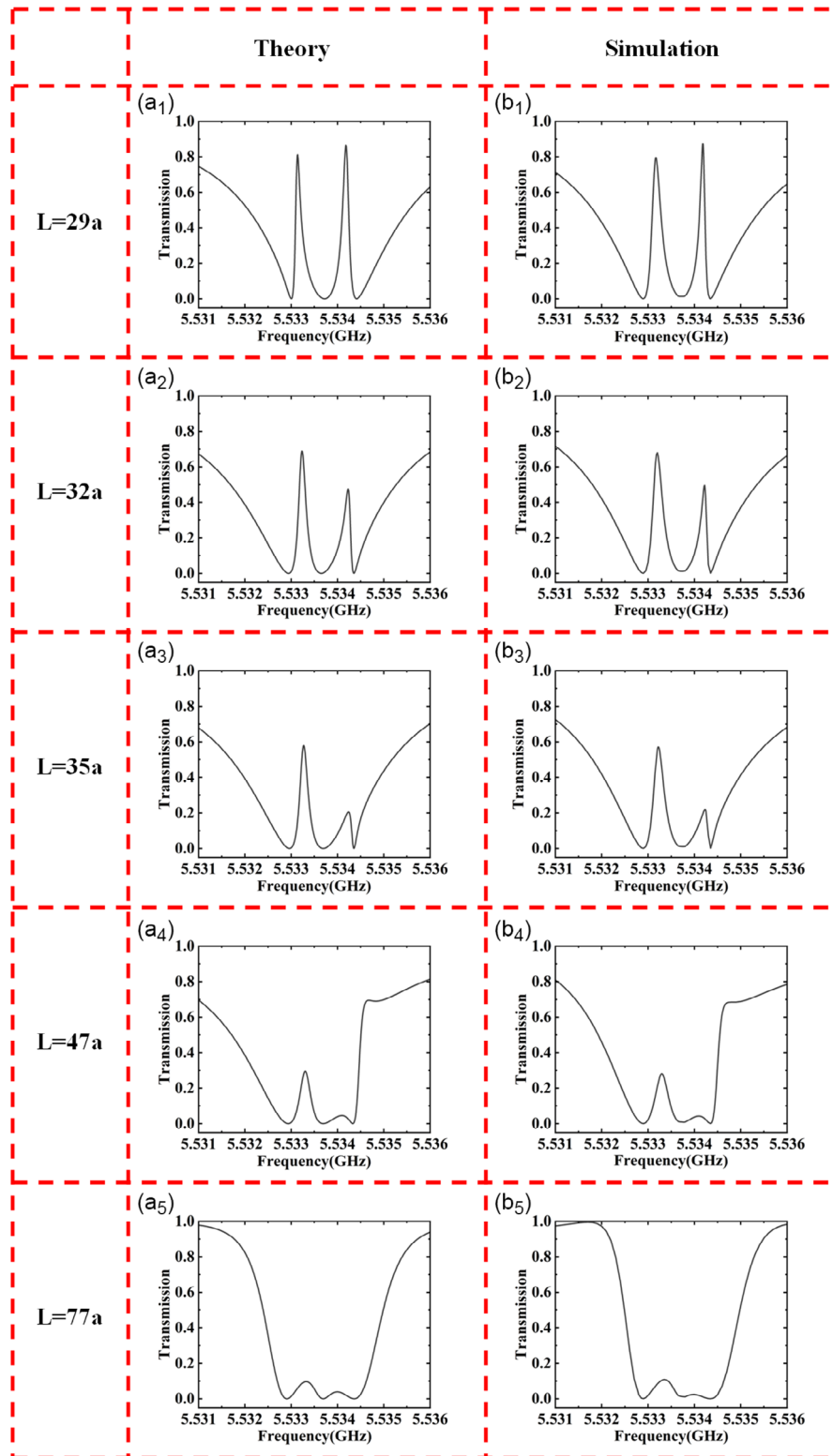


**Figure 4.** a) The theoretical (the first column) and b) simulated (the second column) spectra with different far-field coupling.  $a_1, b_1$ ) The distance between two CS cavities is 29a;  $a_2, b_2$ ) the distance between two CS cavities is 32a;  $a_3, b_3$ ) the distance between two CS cavities is 35a;  $a_4, b_4$ ) the distance between two CS cavities is 47a; and  $a_5, b_5$ ) the distance between two CS cavities is 77a.



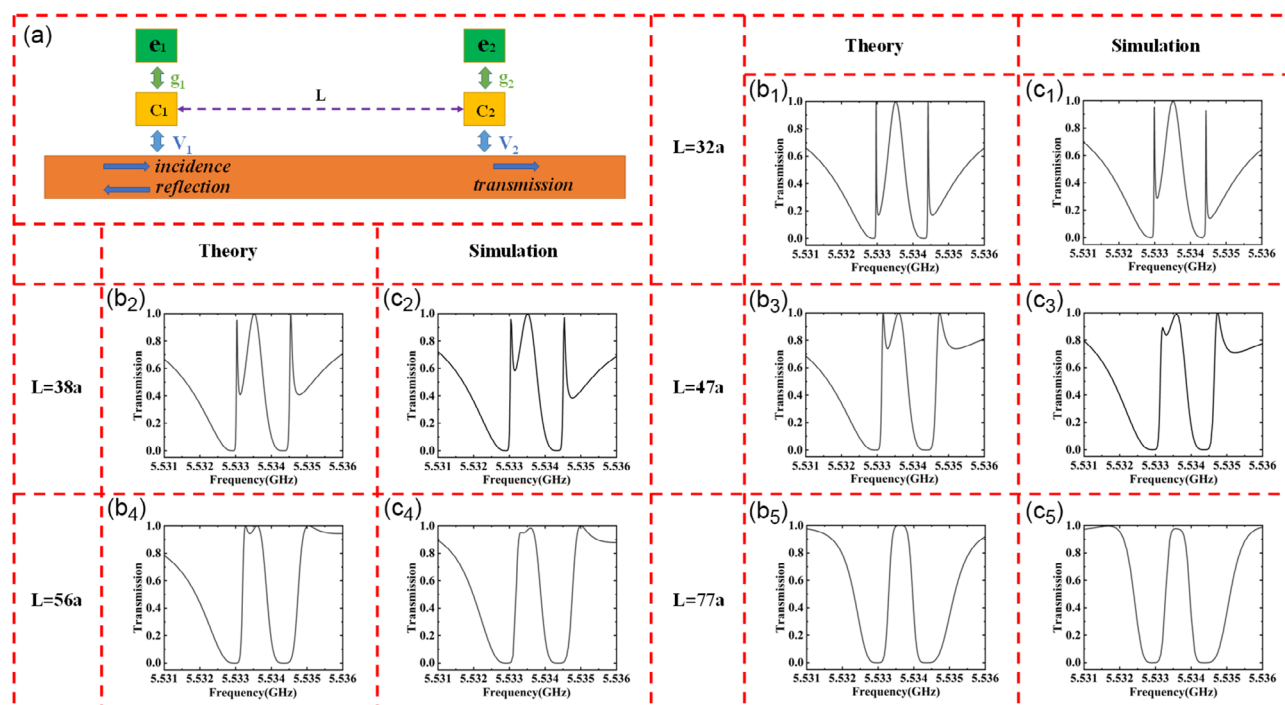


**Figure 5.** a) Theoretical model of the cavity–waveguide system consisting of  $e_1, e_2$  two trival cavities and  $C_1, C_2$  two separated CS cavities coupled by an ES waveguide.  $b_1$ – $c_5$ ) The theoretical (the first column) and simulated (the second column) spectra with different far-field couplings.  $b_1, c_1$ ) The distance between two CS cavities is  $32a$ ;  $b_2, c_2$ ) the distance between two CS cavities is  $38a$ ;  $b_3, c_3$ ) the distance between two CS cavities is  $47a$ ;  $b_4, c_4$ ) the distance between two CS cavities is  $56a$ ; and  $b_5, c_5$ ) the distance between two CS cavities is  $77a$ .

transmission spectrum can be also obtained, as shown in Figure S13, Supporting Information.

## 4. Conclusion and Outlook

In summary, we have proposed an approach for designing cavity–waveguide systems that consists of two separated CS cavities (interacting with one or two trival cavities) coupled by means of an ES waveguide to robustly tune the transmission spectra of EM waves. The far-field coupling, that is, the phase coupling between the two separated CS cavities, instead of traditional near-field coupling was considered as a new degree of freedom to control the propagation characteristics of EM waves. The single-, dual-, and triple-EIT-like transmission spectra with tunable transmissivity (of the transparent peak[s]) were numerically realized. In addition, the robustness in the EIT-like transmission characteristics was also demonstrated. The corresponding theoretical models were constructed to further reveal the tunable properties (of transmission spectra) based on the far-field coupling. The unique method for robustly controlling/tuning the propagation of EM waves in a cavity–waveguide system will open a new window to designing high-performance and ultracompact functional devices in flexibly manipulating EM waves.

## Supporting Information

Supporting Information is available from the Wiley Online Library or from the author.

## Acknowledgements

This work was supported by the National Key Research and Development Program of China (Grant no. 2017YFA0701005), National Natural Science Foundation of China (Grant nos. 62271320 and 61871268), the Science and Technology Commission of Shanghai Municipality (Grant no. 22JC1400200), “Shuguang” Program of Shanghai Education Commission (Grant no. 19SG44), the 111 Project (Grant no. D18014), and the Shanghai Committee of Science and Technology (Grant no. 21S31907400).

## Conflict of Interest

The authors declare no conflict of interest.

## Data Availability Statement

The data that support the findings of this study are available from the corresponding author upon reasonable request.

## Keywords

far-field modulation, nontrivial/trivial modes, phase coupling, tunable property

Received: March 3, 2023  
Revised: April 3, 2023  
Published online: April 21, 2023



- [1] J. D. Joannopoulos, S. G. Johnson, J. N. Winn, R. D. Meade, in *Photonic Crystals: Molding The Flow Of Light*, 2nd ed, Princeton University Press, Princeton **2008**.
- [2] J. Lian, S. Sokolov, E. Yüce, S. Combríe, A. De Rossi, A. P. Mosk, *Phys. Rev. A* **2017**, *96*, 033812.
- [3] Y. An, T. Fu, Q. Liu, Z. B. Ouyang, *Appl. Phys. Express* **2020**, *13*, 032006.
- [4] M. F. Yanik, W. Suh, Z. Wang, S. H. Fan, *Phys. Rev. Lett.* **2004**, *93*, 23390.
- [5] T. Gu, S. Kocaman, X. Yang, J. F. McMillan, M. B. Yu, G.-Q. Lo, D.-L. Kwong, C. W. Wong, *Appl. Phys. Lett.* **2011**, *98*, 121103.
- [6] F. Jiang, C. S. Deng, Q. Lin, L. L. Wang, *Opt. Express* **2019**, *27*, 32122.
- [7] J. Scheuer, *J. Opt. Soc. Am. B-Opt. Phys.* **2016**, *33*, 1827.
- [8] Á. Andueza, J. Pérez-Conde, J. Sevilla, *Opt. Express* **2016**, *24*, 18807.
- [9] J. Romero-Vivas, D. N. Chigrin, A. V. Lavrinenko, C. M. S. Torres, *Opt. Express* **2005**, *13*, 826.
- [10] K. Fasihi, S. Mohammadnejad, *Opt. Express* **2009**, *17*, 8983.
- [11] Y. D. Wu, K. W. Hsu, T. T. Shih, J. J. Lee, *J. Opt. Soc. Am. B-Opt. Phys.* **2009**, *26*, 640.
- [12] J. B. Khurgin, *J. Opt. Soc. Am. B-Opt. Phys.* **2005**, *22*, 1062.
- [13] T. Baba, *Nat. Photon.* **2008**, *2*, 465.
- [14] F. D. M. Haldane, S. Raghu, *Phys. Rev. Lett.* **2008**, *100*, 013904.
- [15] Z. Wang, Y. D. Chong, J. D. Joannopoulos, M. Soljačić, *Phys. Rev. Lett.* **2008**, *100*, 013905.
- [16] M. Hafezi, E. A. Demler, M. D. Lukin, J. M. Taylor, *Nat. Phys.* **2011**, *7*, 907.
- [17] A. B. Khanikaev, S. H. Mousavi, W. K. Tse, M. Kargarian, A. H. MacDonald, G. Shvets, *Nat. Mater.* **2013**, *12*, 233.
- [18] L. Lu, L. Fu, J. D. Joannopoulos, M. Soljacic, *Nat. Photonics* **2013**, *7*, 294.
- [19] A. Slobozhanyuk, S. H. Mousavi, X. Ni, D. Smirnova, Y. S. Kivshar, A. B. Khanikaev, *Nat. Photonics* **2017**, *11*, 130.
- [20] W. A. Benalcazar, B. A. Bernevig, T. L. Hughes, *Science* **2017**, *357*, 61.
- [21] Z. Wang, Y. D. Chong, J. D. Joannopoulos, M. Soljacic, *Nature* **2009**, *461*, 772.
- [22] Y. H. Yang, Z. Gao, H. R. Xue, L. Zhang, M. J. He, Z. J. Yang, R. J. Singh, Y. D. Chong, B. L. Zhang, H. S. Chen, *Nature* **2019**, *565*, 622.
- [23] X. T. He, E. T. Liang, J. J. Yuan, H. Y. Qiu, X. D. Chen, F. L. Zhao, J. W. Dong, *Nat. Commun.* **2019**, *10*, 872.
- [24] L. H. Wu, X. Hu, *Phys. Rev. Lett.* **2015**, *114*, 223901.
- [25] F. Fan, S. Chen, S. J. Chang, *IEEE J. Sel. Top. Quant.* **2017**, *23*, 8500111.
- [26] F. Gao, H. R. Xue, Z. J. Yang, K. F. Lai, Y. Yu, X. Lin, Y. D. Chong, G. Shvets, B. L. Zhang, *Nat. Phys.* **2018**, *14*, 140.
- [27] Q. Y. Mu, F. Fan, S. Chen, S. T. Xu, C. Z. Xiong, X. Zhang, X. H. Wang, S. J. Chang, *Photon. Res.* **2019**, *7*, 325.
- [28] R. Zhou, H. Lin, Y. Liu, X. T. Shi, R. X. Tang, Y. J. Wu, Z. H. Yu, *Phys. Rev. A* **2021**, *104*, L031502.
- [29] B. Yan, Y. C. Peng, A. Q. Shi, J. L. Xie, P. Peng, J. J. Liu, *Opt. Lett.* **2022**, *47*, 2044.
- [30] C. C. Lu, Y. Sun, C. Wang, H. Zhang, W. Zhao, X. Hu, M. Xiao, W. Ding, Y. Liu, C. T. Chan, *Nat. Commun.* **2022**, *13*, 2586.
- [31] M. S. Garcia, V. Peri, R. Süssstrunk, O. R. Bilal, T. Larsen, L. G. Villanueva, S. D. Huber, *Nature* **2018**, *555*, 342.
- [32] C. W. Peterson, W. A. Benalcazar, T. L. Hughes, G. Bahl, *Nature* **2018**, *555*, 346.
- [33] B. Y. Xie, G. X. Su, H. F. Wang, H. Su, X. P. Shen, P. Zhan, M. H. Lu, Z. L. Wang, Y. F. Chen, *Phys. Rev. Lett.* **2019**, *122*, 233903.
- [34] L. He, Z. Addison, E. J. Mele, B. Zhen, *Nat. Commun.* **2020**, *11*, 3119.
- [35] Y. Liu, S. W. Leung, F. F. Li, Z. K. Lin, X. F. Tao, Y. Poo, J. H. Jiang, *Nature* **2021**, *589*, 381.
- [36] R. Chen, C. Z. Chen, J. H. Gao, B. Zhou, D. H. Xu, *Phys. Rev. Lett.* **2020**, *124*, 036803.
- [37] H. H. Qiu, M. Xiao, F. Zhang, C. Y. Qiu, *Phys. Rev. Lett.* **2021**, *127*, 146601.
- [38] J. L. Lu, K. G. Wirth, W. L. Gao, A. Heßler, B. Sain, T. Taubner, T. Zentgraf, *Sci. Adv.* **2021**, *7*, eabl3903.
- [39] R. Zhou, H. Lin, Y. J. Wu, Z. F. Li, Z. H. Yu, Y. Liu, D. H. Xu, *Photon. Res.* **2022**, *10*, 1244.
- [40] P. Peng, E. X. Liu, B. Yan, Y. C. Peng, A. Q. Shi, J. L. Xie, H. Li, Y. J. Xiang, J. J. Liu, *Appl. Phys. Lett.* **2022**, *121*, 011103.
- [41] R. G. Gladstone, M. Jung, G. Shvets, *Phys. Rev. Lett.* **2022**, *128*, 026801.
- [42] J. P. Jiang, B. Yan, Y. C. Peng, J. L. Xie, A. Q. Shi, J. J. Liu, *Opt. Lett.* **2022**, *47*, 437.
- [43] S. S. Yamada, T. Li, M. Lin, C. W. Peterson, T. L. Hughes, G. Bahl, *Nat. Commun.* **2022**, *13*, 2035.
- [44] Y. D. Li, C. X. Fan, X. Y. Hu, Y. T. Ao, C. C. Lu, C. T. Chan, D. M. Kennes, Q. H. Gong, *Phys. Rev. Lett.* **2022**, *129*, 053903.
- [45] Q. X. Xu, Y. C. Peng, B. Yan, A. Q. Shi, P. Peng, J. L. Xie, J. J. Liu, *Opt. Lett.* **2023**, *48*, 101.
- [46] W. A. Benalcazar, B. A. Bernevig, T. L. Hughes, *Phys. Rev. B* **2017**, *96*, 245115.
- [47] W. A. Benalcazar, T. H. Li, T. L. Hughes, *Phys. Rev. B* **2019**, *99*, 245151.
- [48] Y. Ota, F. Liu, R. Katsumi, K. Watanabe, K. Wakabayashi, Y. Arakawa, S. Iwamoto, *Opti≈* **2019**, *6*, 786.
- [49] C. Y. Ji, G. B. Liu, Y. Zhang, B. S. Zou, Y. G. Yao, *Phys. Rev. A* **2019**, *99*, 043801.
- [50] A. Q. Shi, B. Yan, R. Ge, J. L. Xie, Y. C. Peng, H. Li, W. E. I. Sha, J. J. Liu, *Opt. Lett.* **2021**, *46*, 1089.
- [51] J. Xu, X. F. Zang, X. D. Zhan, K. Liu, Y. M. Zhu, *Opt. Lett.* **2022**, *47*, 5204.
- [52] W. Tan, Y. Sun, Z. G. Wang, H. Chen, *Appl. Phys. Lett.* **2014**, *104*, 091107.
- [53] C. F. Fan, F. Wu, Y. H. Li, H. T. Jiang, Y. Sun, H. Chen, *Photon. Res.* **2022**, *10*, 41.
- [54] Y. T. Ao, X. Y. Hu, Y. L. You, C. C. Lu, Y. L. Fu, X. Y. Wang, Q. H. Gong, *Phys. Rev. Lett.* **2020**, *125*, 013902.
- [55] J. S. Tang, W. Nie, L. Tang, M. Y. Chen, X. Su, Y. Q. Lu, F. Nori, K. Y. Xia, *Phys. Rev. Lett.* **2022**, *128*, 203602.